

Functionalization of Polyurethane/Urea Copolymers with Amide Groups by Polymer Treatment with Ammonia Plasma

Alenka Vesel¹ · Rok Zaplotnik¹ · Gregor Primc¹ ·
Xiangyu Liu² · Kaitian Xu² · Kevin C. Chen² ·
Chiju Wei² · Miran Mozetic¹

Received: 14 December 2015 / Accepted: 17 January 2016 / Published online: 27 January 2016
© Springer Science+Business Media New York 2016

Abstract Samples of porous foam from polyurethane/urea copolymers based on polyethylene glycol (PURPEG) were prepared in the form of 1-mm-thick discs of diameter 10 cm and exposed to ammonia plasma created by inductively coupled radiofrequency discharge in either low density (E mode) or high density (H mode). The evolution of surface composition and structure upon plasma treatment was characterized by X-ray photoelectron spectroscopy. Treatment in the H mode caused depletion of oxygen even after 2 s of treatment, whereas treatment in the E mode caused gentle functionalization with amide groups. The concentration of functional groups depended on the discharge power, and the best results were obtained at moderately high power just before the transition from E to H modes.

Keywords Polyurethanes · Polyurea copolymer · Biodegradable · Ammonia plasma treatment · Surface modification · XPS

Introduction

Polymer materials are currently widely used in both science and industrial production [1, 2]. A particular example is biomedicine. A wide variety of simple and more complex polymers are used for synthesis of materials that make contact with biological matter, such as scaffolds for tissue engineering [3, 4]. Of particular interest are biodegradable polymers

Electronic supplementary material The online version of this article (doi:10.1007/s11090-016-9696-3) contains supplementary material, which is available to authorized users.

✉ Alenka Vesel
alenka.vesel@guest.arnes.si

¹ Jozef Stefan Institute, Jamova cesta 39, 1000 Ljubljana, Slovenia

² Multidisciplinary Research Center, Shantou University, Shantou 515063, Guangdong, China

[5–7]. Both synthetic and natural polymers have been investigated as biodegradable polymer materials. Biodegradation of polymeric biomaterials is due to cleavage of hydrolytically or enzymatically sensitive bonds in the polymer, leading to polymer degradation [5]. Depending on the mode of degradation, polymeric biomaterials can be classified as hydrolytically degradable polymers and enzymatically degradable polymers. Synthetic biodegradable polymers include poly(lactic acid), poly(glycolic acid), poly(hydroxybutyrate), poly(ϵ -caprolactone), poly(β -malic acid) and poly(dioxanones) [5, 8, 9]. Although these materials often yield satisfactory results, researchers worldwide are seeking for novel copolymers with outstanding properties.

Regardless of the polymer used for a particular application, the surface properties are often inadequate; thus, they should be modified before application [10–15]. There are several methods for surface modification without changing other properties of treated materials, but treatment by gaseous plasma has often been proved as the best, due to its ability to tailor surface functional groups and its ecological suitability [16–21]. Non-equilibrium plasma is usually applied to prevent any degradation of treated materials due to thermal effects. Both atmospheric- and low-pressure discharges are used for plasma-induced modifications of polymer materials. The advantages of atmospheric plasma are the low price of the plasma system and the ability of streamers to propagate through porous materials. Low-pressure plasma, however, can be very homogeneous in large volumes; therefore, it is suitable for treatment of three-dimensional objects with complex geometry. The penetration of charged particles through porous polymers is limited; however, neutral reactive particles that usually prevail in low-pressure plasma can penetrate deep into porous polymer structures if a pressure gradient is applied across the materials [22].

The type of functional groups established on a polymer surface upon plasma treatment depends on numerous parameters. Gaseous plasma is rich in both charged and neutral reactive particles, and radiation in a broad range from infrared to ultraviolet is usually present as well [23]. The reactive particles interact with polymer surfaces, and the chemical reactions are usually exothermic. Polymer materials of low thermal conductivity such as porous ones are therefore heated upon plasma treatment, although the neutral gas kinetic temperature in plasma is near room temperature. Plasma treatment of a polymer causes both functionalization and etching [24–29]. The surface functional groups may therefore be unstable and desorb from the surface before becoming detectable by available methods for surface characterization.

An important consideration in any attempt to use plasma technology on an industrial scale is the duration of the processing. Many materials are produced online in the continuous mode; thus, the feasible plasma treatment time is limited, typically to only a few seconds. Otherwise, any online plasma treatment would require very long reactors that are impractical. The treatment should thus result in the required surface finish after a few seconds of plasma treatment.

Plasma can be sustained by various gaseous discharges. Often, an inductively coupled RF generator is used. Such a discharge configuration has some advantages over other types of gaseous discharges; the main one is the absence of electrodes in the plasma chamber and thus absence of pollution of samples with material that might be sputtered from the electrodes upon bombardment with positive ions [30]. Inductively coupled discharges create plasma in two distinct modes: E or H mode. At low discharge power, plasma is always in the E mode because the heating of plasma electrons by an induced electric field inside the RF coil is negligible compared with heating in the sheath next to dielectric surfaces backed by the powered side of the RF coil. Once the power increases over a threshold, a transition to the H mode occurs. The E mode is dominated by capacitive

coupling, and plasma often spreads over the entire discharge chamber. This is characterized by weak light emission, low electron density, moderate neutral atom density and relatively high electron temperature [31, 35]. In contrast, the H mode is purely inductive and characterized by strong light intensity concentrated in a rather small volume, high electron and neutral atom density, and somewhat lower electron temperature. The RF power where transition occurs depends on pressure [31]. The transition between the modes is abrupt at moderately high pressures [31–33] and less pronounced at pressures below, say, 1 Pa [34]. Several authors have reported hysteresis or even instabilities at the transition [36, 37]. The hysteresis has been explained by considering possible nonlinear mechanisms for sustaining the plasma. Characterization of plasma at the transition from E to H modes is not a trivial task due to high-frequency interference and different orders of magnitude in electron density. OES tomography is one of the best methods [38, 39], and cutoff probes perform well if the electron density is below approximately $1 \times 10^{18} \text{ m}^{-3}$ [34].

In this study, we report our findings on the surface modification of biodegradable polyurethane/ureas using ammonia gas plasma treatment in E and H modes.

Experimental Procedure

Materials

Poly(ethylene glycol) (PEG) (MW 2000) was obtained from Sigma-Aldrich; 4,4'-methylene bis(cyclohexyl isocyanate) (HMDI) was obtained from Alfa-Aesar; 4,4'-diaminodicyclohexylmethane (PACM) was obtained from Yexu Industry Co. Ltd. (Shenzhen, China); 1,2-dichloromethane (AR grade) and sodium chloride were purchased from YongDa Reagent Development Center (Tianjin, China). The solvent 1,2-dichloromethane was distilled over CaH_2 and stored over a 4A molecular sieve before use.

Synthesis of Polyurea (PURPEG2000) Copolymers

Preparation of Prepolymer PEG-Diisocyanate

An amount of 0.0010 mol PEG (MW 2000) was dissolved in 25 mL of 1,2-dichloroethane, then heated to 115 °C to remove the infinitesimal water in solvent by azeotropic distillation and reduce the amount of solvent to 15 mL. This solution was added dropwise to a 100 mL 4-neck flask in which a slight excess of diisocyanate HMDI (0.0022 mol) was placed in advance. The reaction was carried out at 50 °C for 36 h under a nitrogen atmosphere. The excess HMDI was removed through vacuum distillation using a short partial distillation apparatus operating at 50 °C and a pressure of 1×10^{-2} mbar. After removing HMDI, 5 mL of 1,2-dichloroethane was added to the flask. This PEG-diisocyanate 1,2-dichloroethane solution was kept in the flask and used directly for the next-step reaction [40].

Synthesis of the PURPEG2000 Polymers and the Film

Polyurea PURPEG2000 was synthesized via the coupling reaction of 4,4'-diaminodicyclohexylmethane (PACM) and a terminal diisocyanate group ending with PEG—i.e., PEG-diisocyanate at an equal molar ratio. An amount of 0.0010 mol PEG-diisocyanate was

diluted in 30 mL of 1,2-dichloroethane and stirred evenly. The PACM (0.22 mL) was quickly added dropwise to PEG-diisocyanate solution and well stirred quickly, then the solution was poured into glass culture dishes that were placed in an oven and maintained at a constant temperature of 55 °C for 2 days to remove the solvent.

Preparation of PURPEG2000 Foam

An amount of 0.0010 mol PEG-diisocyanate was diluted in 40 mL of 1,2-dichloroethane and stirred evenly. Twelve grams of dried sodium chloride particles (40–60 μm) used as porogen for the foams was added into the solution and homogenized. The PACM (0.22 mL) was quickly added dropwise to PEG-diisocyanate solution and quickly stirred, and then, the solution was poured into two glass culture dishes that were placed in an oven and maintained at a constant temperature of 55 °C for 2 days to remove the solvent. The dishes were placed in ultrapure water to remove the porogen from the polymer films. After removing the NaCl particles, the materials full of water were frozen at –20 °C and then placed into a lyophilizer for 48 h to form the porous foam [41]. The structural formula of the synthesized material is presented in Fig. 1.

Plasma Treatment

Samples were cut into small pieces of size approximately 1 cm² and exposed to gaseous plasma. The plasma chamber was a borosilicate glass tube of inner diameter 3.6 cm. The system was pumped on one side with a two-stage rotary pump of nominal pumping speed 80 m³/h, and on other side, ammonia of commercial purity 99.9 % was leaked through a leak valve. The gas pressure in the plasma chamber was therefore constant due to continuous gas leaking and pumping and was fixed at 50 Pa for these particular experiments. The rather powerful vacuum pump allowed for rapid removal of any reaction products that might otherwise cause changes in the plasma characteristics. Plasma was created by a radiofrequency (RF) discharge and was characterized by optical emission spectroscopy using an AVANTES AvaSpec-3648 spectrometer with 0.5 nm resolution in the wavelength range from 200 to 1100 nm.

The RF generator was coupled to a copper coil and placed at the center of the plasma chamber via a matching network. The RF generator operated at the standard industrial frequency of 13.56 MHz and adjustable forward power up to 1200 W. The generator was also equipped with a detector of reflected power. The reflected power depended on the adjustment of two variable capacitors in the matching network. The network was fixed such that the reflected power was minimal in the H mode, and it was mismatched in the E mode [31]. The plasma treatment of polymer samples was conducted at various forward power levels up to 800 W. At these particular conditions, the transition from E to H mode appeared at the forward power of approximately 350 W. Plasma was unstable between 350 and 500 W, after which it was in the H mode. The transition was abrupt and easily observable with the naked eye because the luminosity of plasma in the H mode was approximately 1000 times larger than in the E mode.

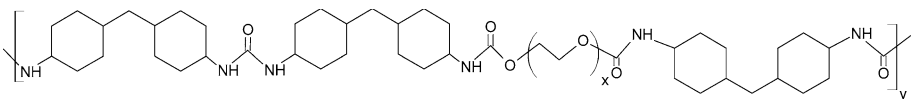


Fig. 1 Structural formula of the synthesized material (PURPEG)

Surface Characterization

Samples were characterized by scanning electron microscopy (SEM) and X-ray photoelectron spectroscopy (XPS). We used an XPS instrument, the TFA XPS from Physical Electronics (München, Germany). The samples were excited with monochromatic Al $K_{\alpha 1,2}$ radiation at 1486.6 eV over an area of $400 \mu\text{m}^2$. Photoelectrons were detected with a hemispherical analyzer positioned at an angle of 45° with respect to the normal of the sample surface. XPS survey spectra were measured at a pass-energy of 187 eV using an energy step of 0.4 eV, and high-resolution spectra were measured at a pass-energy of 23.5 eV using an energy step of 0.1 eV. An additional electron gun was used for surface neutralization during XPS measurements. All spectra were referenced to the main C1s peak. The measured spectra were analyzed using MultiPak v8.1c software (Ulvac-Phi Inc., Kanagawa, Japan, 2006) from Physical Electronics, which was supplied with the spectrometer.

Before SEM characterization, the samples were coated with a thin layer of gold. For gold evaporation, a PECS instrument (Model 682) from Gatan GmbH (München, Germany) was used. SEM analyses were performed using a JEOL JSM-840 scanning electron microscope (JEOL, Tokyo, Japan).

Results and Discussion

As-prepared and plasma-treated samples were characterized by SEM. Figure 2 reveals a typical image at a rather low magnification and confirms the highly porous nature of the synthesized samples. The porosity was approximately 70 %, whereas the surface and interior pore size was 30–90 and 70–130 μm . The images of plasma-treated samples did not reveal any significant modification and therefore are not presented.

Plasma was characterized by optical emission spectroscopy. Figure 3 shows a spectrum at the forward power of 300 W (E mode), and Fig. 4 is at 700 W (H mode). Different integration times (E mode, 10 s; H mode, 0.5 ms) were used for the modes because the

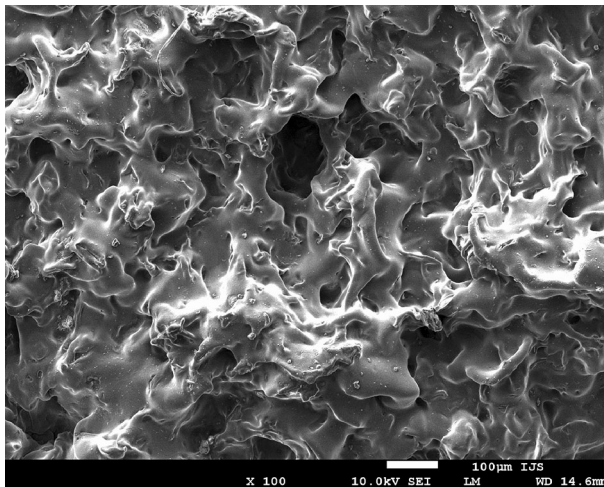


Fig. 2 A typical SEM image of an untreated PURPEG sample

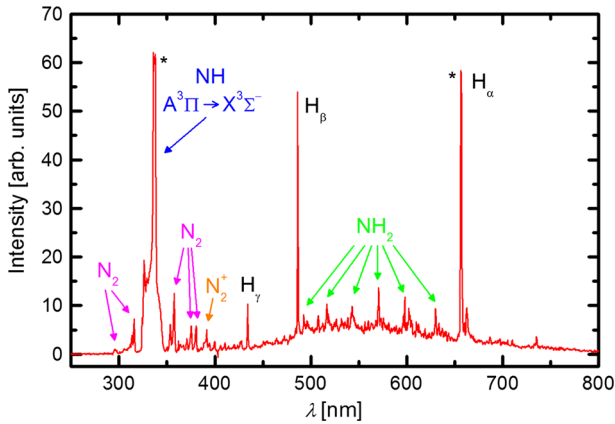


Fig. 3 An optical spectrum of ammonia plasma in E mode at forward power of 300 W. The integration time was 10 s, and the saturated peaks are marked with an *asterisk*

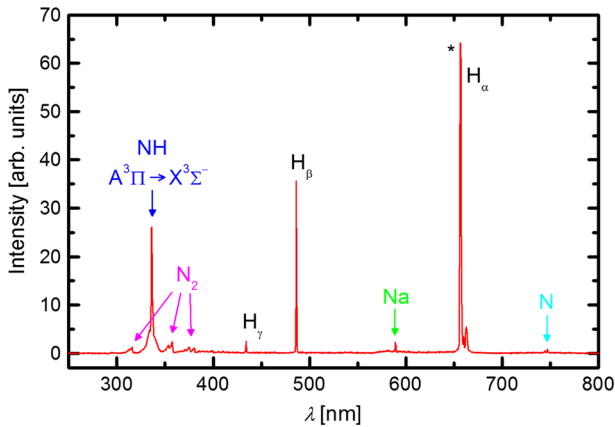


Fig. 4 An optical spectrum of ammonia plasma in H mode at forward power of 700 W. The integration time was 0.5 ms

plasma luminosity changes dramatically at the transition from one mode to the other. In addition to the hydrogen atom Balmer series, the key spectral feature in the E mode is also a very intensive peak in the UV range at 336 nm. In fact, it was left to saturation, the same as H_{α} , to make the other spectral features more pronounced. This peak at 336 nm corresponds to the transition of the NH radical. There is also radiation that arises from the transition of neutral nitrogen molecule in the UV part of the spectrum with the largest peak at 337.1 nm, which corresponds to the $C^3\Pi_u \rightarrow B^3\Pi_g(0,0)$ transition and spectrally overlaps with the NH band; the second largest peak is at 357.7 nm, which corresponds to the $C^3\Pi_u \rightarrow B^3\Pi_g(0,1)$ transition. This observation indicates the appearance of nitrogen molecules in plasma, probably due to surface recombination of nitrogen atoms. The rich bands in the broad range from approximately 450–650 nm originate in transitions from excited NH_2 radicals. The technique is qualitative, so the spectra indicate only that the ammonia molecules are extensively dissociated from NH and NH_2 radicals. The absence of

emission arising from radiative transition of N atoms (the major line should appear in the red part of the spectrum at approximately 746 nm), however, indicates that the full dissociation of ammonia molecules to parent atoms is a rare event in the E mode.

The spectrum for the H mode presented in Fig. 4 is much different. In this case, the H_α peak was also left to saturation. Here, it is worth mentioning that in the H mode, the H_α peak is approximately 3.5 times higher than the H_β peak, whereas in the E mode, this ratio is approximately 1.5. This is due to the different electron temperatures in E and H modes. The electron temperature in the E mode is larger than that in the H mode. The radiation from NH_2 is absent, which is a qualitative confirmation for a very low concentration of this radical in the H mode. The NH line at 336 nm still persists but is less intensive than the H_β line, and therefore, the concentration of this radical compared with other reactive species such as H and N is obviously much lower in the H than in the E mode. The rather weak nitrogen band also indicates that nitrogen molecules formed by surface recombination dissociate in the plasma. Although the nitrogen atomic lines are rarely observed in low-pressure non-equilibrium plasma due to the high excitation energy of the radiative state, the transitions $4S^\circ 3/2 \rightarrow 4P 5/2$, $4S^\circ 3/2 \rightarrow 4P 3/2$ and $4S^\circ 3/2 \rightarrow 4P 1/2$ are clearly distinguished with three lines at 746.8, 744.2 and 742.3 nm, respectively.

The optical spectra shown in Figs. 3 and 4, therefore, indicate partial dissociation of NH_3 molecules into NH and NH_2 radicals in the E mode, whereas ammonia is almost fully dissociated to parent atoms in the H mode.

Samples were treated in ammonia plasma at various conditions and then characterized by XPS. Untreated sample was composed of approximately 1.4 atomic percent (at.%) of nitrogen and 18.2 at.% oxygen, and the remainder was carbon (see also the figure in Online Resource Fig. S1). The spectra were acquired at different positions on the surface, and the calculated composition varied by approximately 10 %, which is typical for such porous copolymers.

Samples were placed into the plasma chamber in the middle of the copper coil where the plasma luminosity was largest. Figure 5 reveals the surface composition versus power. Figure 5 is plotted against real power (P_{real}), whereas forward power ($P_{Forward}$) is marked next to the measured points. The real power was estimated by subtracting the reflected power from the forward power. The values up to $P_{real} = 70$ W ($P_{Forward} = 300$ W) correspond to plasma in the E mode, whereas the value of $P_{real} = 90$ W ($P_{Forward} = 350$ W)

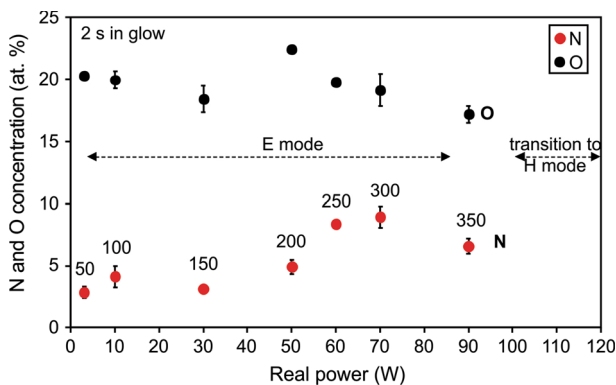


Fig. 5 The concentration of nitrogen and oxygen versus real power for the case of samples mounted in the center of the RF coil. The treatment time was 2 s. The values next to the measured points represent forward power

corresponds to unstable plasma of frequent transitions from E to H modes. The nitrogen concentration increases with increasing discharge power as long as plasma is in the E mode up to $P_{real} = 70$ W ($P_{Forward} = 300$ W). As mentioned earlier, the coupling is mismatched in the E mode, and the reflected power is high. For the sample treated at the transition to the H mode, a sudden reduction of nitrogen concentration is observed. Furthermore, thermal degradation was observed with the naked eye, which was explained by extensive surface exothermic reactions. The H mode is therefore inappropriate for surface modification of this copolymer even for treatment times as low as 2 s.

To reveal the influence of powerful plasma but preserve the samples, they were also treated at the edge of the coil where the plasma luminosity was not very extensive. Samples were placed 2 cm from the coil in the direction towards the pump. At this position, the electron density is much lower than inside the coil, but the density of neutral reactive particles is almost as high as that within the coil. The concentration of nitrogen in the surface of the polymer samples as determined by XPS versus real discharge power for samples treated at the edge of the coil is shown in Fig. 6, and the concentration of oxygen is given in Fig. 7. The forward discharge power is marked next to the measured points. One can observe a sudden increase in nitrogen concentration and simultaneous decrease in oxygen concentration as plasma transforms from E to H mode. The samples were not degraded visually; thus, treatment at the edge of the H mode plasma seems suitable for functionalization. However, the extensive oxygen depletion indicates important degradation of the surface film, probably due to interaction with reactive hydrogen species. Therefore, treatment in the H mode is less suitable for rapid functionalization without modification of other properties than treatment in the E mode inside the RF coil.

Appearance of the nitrogen functional groups upon plasma treatment was therefore elaborated for samples placed into the center of the RF coil for 2 s in the E mode. Figure 8 reveals the evolution of the high resolution C1 s peaks upon plasma treatment. Apart from the increased peak (#2) at 286.3 eV, the major change in the peak occurs at a high binding energy—i.e., greater than approximately 288 eV (#3, #4). Peak #1, of course, corresponds to C–C and C–H bonds. To gain insight into the types of groups formed on the polymer surface that contribute to the appearance of the peaks #2–4, selected peaks were deconvoluted. Figure 9a shows the deconvoluted C1s peak for an untreated sample, Fig. 9b for

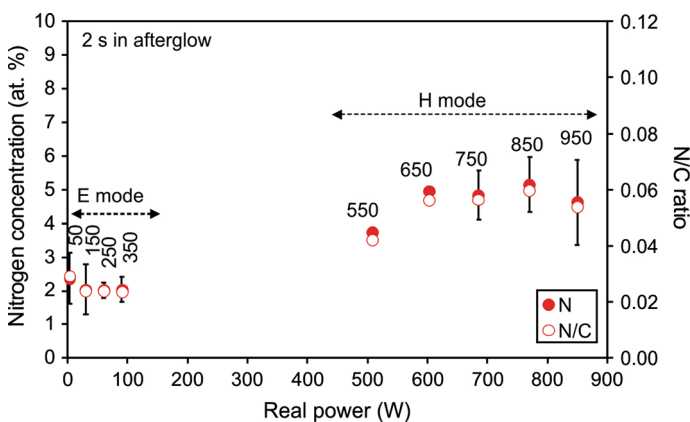


Fig. 6 The concentration of nitrogen versus real power for the case of samples mounted at the edge of the RF coil. The treatment time was 2 s. The values next to the measured points represent forward power

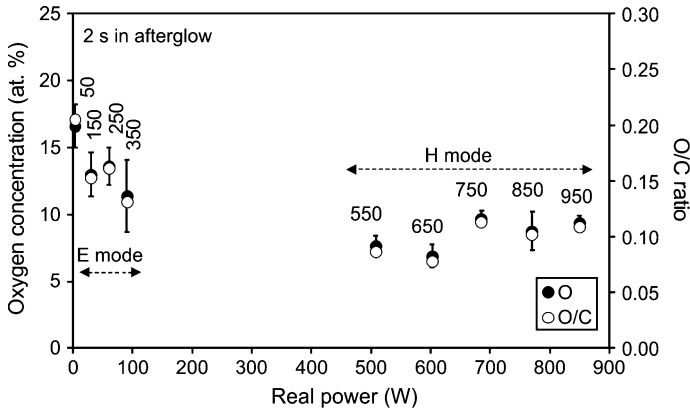
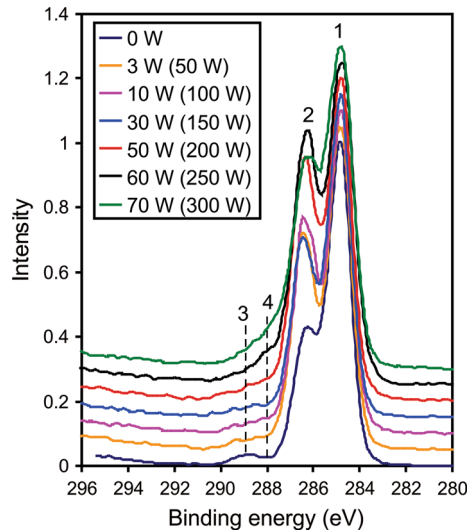


Fig. 7 The concentration of oxygen versus real power for the case of samples mounted at the edge of the RF coil. The treatment time was 2 s. The values next to the measured points represent forward power

Fig. 8 The high-resolution C1 s peaks for PURPEG samples treated in the center of the RF coil for 2 s versus real power (corresponding forward power is shown in brackets)



the sample treated at the $P_{real} = 3\text{ W}$ ($P_{Forward} = 50\text{ W}$), and Fig. 9c for $P_{real} = 70\text{ W}$ ($P_{Forward} = 300\text{ W}$). The concentration of different bonds is summarized in Table 1.

Figure 9a reveals the binding of carbon atoms in the as-synthesized sample. Although the monomer unit contains only one -NH-CO-O- and one -NH-CO-NH- unit (urethane and urea group), they are observable at the high-energy tail of the C1s peak at approximately 289 eV. Other functionalities cannot be revealed from the C1s peak because the C–O and C–N practically overlap with binding energy of approximately 286.3 eV and 285.8 eV, respectively. The concentration of nitrogen, however, is small on the surface of the untreated samples at $<2\text{ at.}\%$; thus, one can attribute the well-pronounced peak at 286.3 eV predominantly to the C–O functional group. According to the chemical structure presented in Fig. 1, the C–O group arises from the polyethylene chain of the PEG

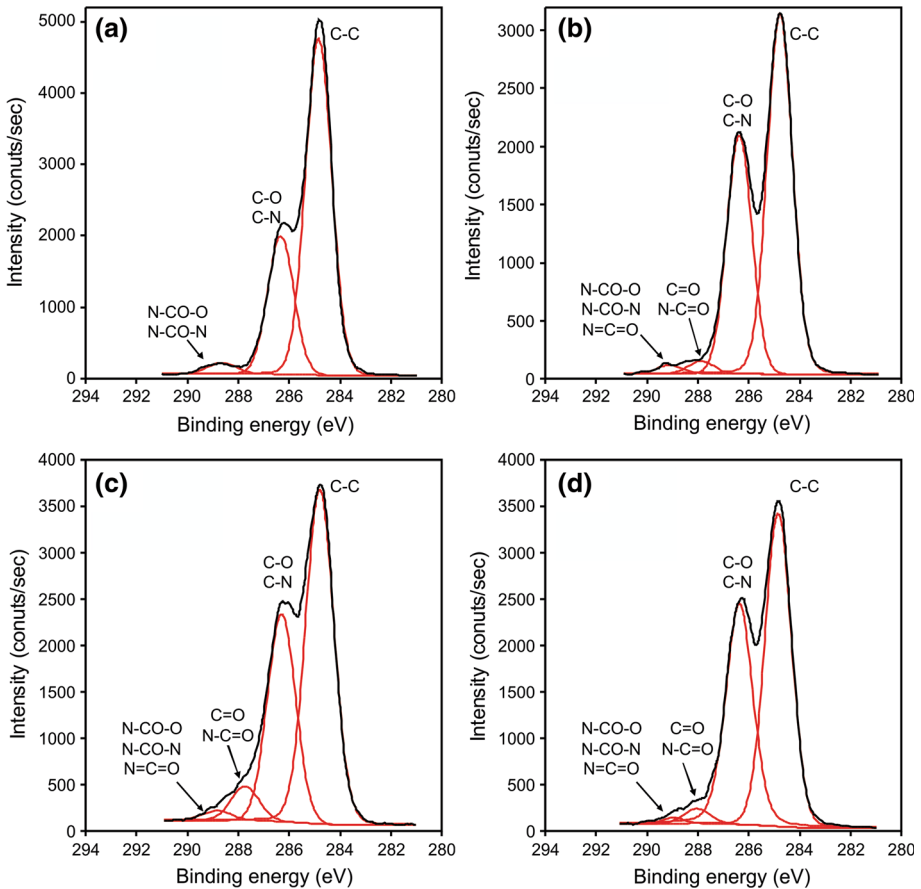


Fig. 9 Best deconvolution of the C1 s peak of the: **a** untreated PURPEG sample, **b** PURPEG sample treated in NH_3 plasma for 2 s at real power of 3 W ($P_{\text{Forward}} = 50$ W), **c** PURPEG sample treated in NH_3 plasma for 2 s at real power of 70 W ($P_{\text{Forward}} = 300$ W) and **d** PURPEG sample treated in NH_3 plasma for 15 s at real power of 3 W ($P_{\text{Forward}} = 50$ W)

Table 1 Concentration of chemical groups of PURPEG samples at different treatment conditions in ammonia plasma (%)

Sample	Peak #1 (248.8 eV) C–C/C–H	Peak #2 (286.3 eV) C–O/C–N	Peak #4 (~288 eV) C = O/N–C=O	Peak #3 (~289 eV) N–CO–O/N–CO–N N = C=O
Untreated	69.5	28.0		2.5
2 s, 3 W	59.0	37.6	2.0	1.4
2 s, 70 W	57.9	34.7	5.7	1.7
15 s, 3 W	55.9	39.9	2.9	1.3

precursor. The total area of the main C–C peak at 284.8 eV in Fig. 9a is 69.5 %; the area of the peak at 286.3 eV (C–O and C–N) is 28 %, whereas the area of the peak at 289 eV (–NH–CO–O– and –NH–CO–NH– groups) is 2.5 % (Table 1).

Treatment of the polymer for 2 s at $P_{real} = 3$ W ($P_{Forward} = 50$ W) reveals some modifications in the surface functionalities. The corresponding C1 s peak is deconvoluted in Fig. 9b. The quantitative analysis reveals that the peak at 286.3 eV represents 38 % of the total C1 s peak. The amount of the high-energy peak at 289 eV decreased slightly, and a new peak at approximately 288 eV appeared. Considering the initial sample surface composition (as revealed from the XPS survey spectrum shown in Online Resource Fig. S1), one can attribute the increase of the peak at 286.3 eV to functionalization of carbon from the aromatic part of the monomer with nitrogen atoms to enrich the surface with C–N groups. This conclusion is sound with results of functionalization of highly aromatic polymers such as polyethylene terephthalate with ammonia plasma [42]. Another possibility would be functionalization of the carbon between two aromatic rings. Any functionalization of the ethylene chain from PEG would not lead to increased area of the peak at 286.3 eV because the carbon atoms in the chain are already bonded to an oxygen atom. In any case, the functionalization is not dramatic, but one should consider the final investigation depth of XPS, which is several nanometers for most polymer materials. The surface is therefore functionalized with additional C–N groups, even when using very low discharge power. As already stressed, 50 W is only the forward power; the real power is rather only 3 W as long as the reflected power meter is trusted.

The decreased intensity of groups –NH–CO–NH– and –NH–CO–O– at 289 eV in Fig. 9b compared with Fig. 9a suggests the destruction of these groups [43, 44]. Namely, it is known that the urethane group can undergo thermal degradation: $R-NH-CO-O-R \rightarrow R-NH_2 + CO_2$ or $R-NH-CO-O-R \rightarrow R-N=C=O + HO-R$ [44]. Similarly, we can expect destruction of urea group to $R-NHCOH + NH_2-R$. Therefore, the formation of isocyanate groups $N=C=O$ or even urea groups $N-CO-N$ may occur. Unfortunately, the difference in their binding energy is too low to distinguish them [45–47]. Therefore, the decrease of the peak at 289 eV from 2.5 % (for the untreated sample, Fig. 9a) to 1.4 % (for the sample treated at $P_{real} = 3$ W, Fig. 9b) indicates at least partial destruction of these groups (Table 1).

Treatment with ammonia plasma also caused another modification of the polymer, leading to surface rearrangement and formation of new functional groups. Figure 8 reveals a gradual increase of the high-energy shoulder with increasing power (see dashed line 4). The best deconvolution as performed in Fig. 9b suggests the appearance of a new peak at 288 eV. This peak could correspond either to carbonyl (C=O) or amide (O=C–N) groups. Because the treatment was performed in an oxygen-free atmosphere, the formation of amide groups is more likely.

Treatment of the polymer at much larger powers reveals a gradual increase of the amide group. Figure 9c shows the deconvoluted C1s peak for the sample treated for 2 s at $P_{real} = 70$ W ($P_{Forward} = 300$ W). The area belonging to the amide group is almost 6 % (Table 1). The peak at 289 eV remains fairly unaffected compared with lower powers, and the increase of the amide groups corresponds to the decrease of the peak at 286.3 eV. Considering the composition of the PURPEG, one can conclude that nitrogen is bonded to the ethylene chain of the monomer unit to form amide groups.

Surface modifications of the PURPEG material upon ammonia plasma treatment for a short period of 2 s in the E mode could thus be summarized as follows: weak plasma causes predominant formation of the amine group, and increased plasma power causes additional functionalization with the amide group. Although high treatment times are unsuitable for treatment of materials in continuous production mode, we checked whether prolonged treatment at low power causes a gradual increase of the amide group. Samples were exposed for 15 s to plasma in the E mode at the real power of 3 W

($P_{Forward} = 50$ W), and XPS characterization was performed. Figure 9d depicts the high-resolution C1s peak for this sample. There is no noteworthy difference compared with the sample treated for 2 s (Fig. 9b; Table 1). Similar results were also observed at other treatment times. This observation indicates the importance of the discharge power on functionalization with specific functional groups. The higher power causes several increasing plasma parameters; thus, the results cannot reveal the exact mechanisms of amide group formation. A feasible explanation would be a strong increase in the UV radiation with increasing real power. According to this hypothesis, the UV radiation arising from both NH transition and hydrogen Lyman series causes bond scission and thus suitable modification for nitridization of the ethylene chain.

Plasma treatment often causes changes in surface free energy, especially when moderately hydrophobic polymers are treated by oxygen plasma [48]. Polymer chain scission produces molecular fragments that often rearrange to form small globules to minimize the surface energy. Such modifications are beneficial in specific applications but may be unwanted in others. To check for any changes in surface energy, we used the standard water drop technique. Droplets of Milli-Q water were deposited onto untreated samples and samples treated in ammonia plasma at various conditions, but the changes in water drop contact angle were marginal—less than 3° , which is within the experimental error. The measurements therefore confirm rather marginal changes in surface wettability.

Conclusions

Polyurea copolymers were treated in low-pressure ammonia plasma to study the formation of different nitrogen-containing functional groups. Powerful plasma in the H mode created by RF discharge at forward powers above 500 W caused a substantial decrease in the oxygen concentration, indicating significant structural changes. The treatment in the E mode was not very destructive and led to rather gentle functionalization. Even very low discharge power, which was estimated to be several watts, led to saturation of the material surface only with amino groups, which was explained by interaction of NH or NH_2 radicals with carbon atoms either within the aromatic rings or adjoining the rings. More powerful plasma caused increased functionalization with the amide groups, probably by interaction with C–O–C groups from the ethylene chains. The rather short treatment time of 2 s makes the plasma treatment suitable for application upon synthesizing materials in the continuous process.

Acknowledgments The research was funded by Slovenian Research Agency ARRS (Project Grant No. L2-6767) and the National Science Foundation of China (NSFC Project No. 21274083) and bilateral project Bi-CN-10-01 and 10-1 (2014).

References

1. John MJ, Thomas S (2008) Biofibres and biocomposites. *Carbohydr Polym* 71(3):343–364. doi:10.1016/j.carbpol.2007.05.040
2. Izdebska J, Thomas S (2016) *Printing on polymers: fundamentals and applications*. Elsevier, Waltham
3. Augustine R, Rajendran R, Cvelbar U, Mozetic M, George A (2013) Biopolymers for health, food, and cosmetic applications. In: *Handbook of biopolymer-based materials*. Wiley-VCH Verlag, pp 801–849. doi:10.1002/9783527652457.ch27
4. Augustine R, Kalarikkal N, Thomas S (2014) Advancement of wound care from grafts to bioengineered smart skin substitutes. *Prog Biomater* 3(2–4):103–113. doi:10.1007/s40204-014-0030-y

5. Nair LS, Laurencin CT (2007) Biodegradable polymers as biomaterials. *Prog Polym Sci* 32(8–9):762–798. doi:[10.1016/j.progpolymsci.2007.05.017](https://doi.org/10.1016/j.progpolymsci.2007.05.017)
6. Ulery BD, Nair LS, Laurencin CT (2011) Biomedical applications of biodegradable polymers. *J Polym Sci B Polym Phys* 49(12):832–864. doi:[10.1002/polb.22259](https://doi.org/10.1002/polb.22259)
7. Mohanty AK, Misra M, Hinrichsen G (2000) Biofibres, biodegradable polymers and biocomposites: an overview. *Macromol Mater Eng* 276(3–4):1–24. doi:[10.1002/\(Sici\)1439-2054\(20000301\)276:1<1:Aid-Mame1>3.0.Co;2-W](https://doi.org/10.1002/(Sici)1439-2054(20000301)276:1<1:Aid-Mame1>3.0.Co;2-W)
8. Augustine R, Dominic EA, Reju I, Kaimal B, Kalarikkal N, Thomas S (2015) Electrospun poly(ϵ -caprolactone)-based skin substitutes: in vivo evaluation of wound healing and the mechanism of cell proliferation. *J Biomed Mater Res B* 103(7):1445–1454. doi:[10.1002/jbm.b.33325](https://doi.org/10.1002/jbm.b.33325)
9. Augustine R, Kalarikkal N, Thomas S (2015) Clogging free electrospinning of polycaprolactone using acetic acid/acetone mixture. *Polym Plast Technol*. doi:[10.1080/03602559.2015.1036451](https://doi.org/10.1080/03602559.2015.1036451)
10. Ferreira P, Alves P, Coimbra P, Gil MH (2015) Improving polymeric surfaces for biomedical applications: a review. *J Coat Technol Res* 12(3):463–475. doi:[10.1007/s11998-015-9658-3](https://doi.org/10.1007/s11998-015-9658-3)
11. Popelka A, Novak I, Lehocky M, Junkar I, Mozetic M, Kleinova A, Janigova I, Slouf M, Bilek F, Chodak I (2012) A new route for chitosan immobilization onto polyethylene surface. *Carbohydr Polym* 90(4):1501–1508. doi:[10.1016/j.carbpol.2012.07.021](https://doi.org/10.1016/j.carbpol.2012.07.021)
12. Popelka A, Novak I, Lehocky M, Chodak I, Sedliacik J, Gajtanska M, Sedliacikova M, Vesel A, Junkar I, Kleinova A, Spirkova M, Bilek F (2012) Anti-bacterial treatment of polyethylene by cold plasma for medical purposes. *Molecules* 17(1):762–785. doi:[10.3390/molecules17010762](https://doi.org/10.3390/molecules17010762)
13. Asadinezhad A, Novak I, Lehocky M, Sedlarik V, Vesel A, Junkar I, Saha P, Chodak I (2010) A physicochemical approach to render antibacterial surfaces on plasma-treated medical-grade PVC: irgasan coating. *Plasma Process Polym* 7(6):504–514. doi:[10.1002/ppap.200900132](https://doi.org/10.1002/ppap.200900132)
14. Lehocky M, Mracek A (2006) Improvement of dye adsorption on synthetic polyester fibers by low temperature plasma pre-treatment. *Czechoslov J Phys* 56:B1277–B1282. doi:[10.1007/s10582-006-0362-5](https://doi.org/10.1007/s10582-006-0362-5)
15. Augustine R, Saha A, Jayachandran VP, Thomas S, Kalarikkal N (2015) Dose-dependent effects of gamma irradiation on the materials properties and cell proliferation of electrospun polycaprolactone tissue engineering scaffolds. *Int J Polym Mater Polym Biomater* 64(10):526–533. doi:[10.1080/00914037.2014.977900](https://doi.org/10.1080/00914037.2014.977900)
16. Morent R, De Geyter N, Desmet T, Dubruel P, Leys C (2011) Plasma surface modification of biodegradable polymers: a review. *Plasma Process Polym* 8(3):171–190. doi:[10.1002/ppap.201000153](https://doi.org/10.1002/ppap.201000153)
17. Vesel A, Junkar I, Cvelbar U, Kovac J, Mozetic M (2008) Surface modification of polyester by oxygen- and nitrogen-plasma treatment. *Surf Interface Anal* 40(11):1444–1453. doi:[10.1002/sia.2923](https://doi.org/10.1002/sia.2923)
18. Chu PK, Chen JY, Wang LP, Huang N (2002) Plasma-surface modification of biomaterials. *Mater Sci Eng R* 36(5–6):143–206. doi:[10.1016/S0927-796X\(02\)00004-9](https://doi.org/10.1016/S0927-796X(02)00004-9)
19. Vesel A (2008) XPS study of surface modification of different polymer materials by oxygen plasma treatment. *Inf Midem* 38(4):257–265
20. Jacobs T, Morent R, De Geyter N, Dubruel P, Leys C (2012) Plasma surface modification of biomedical polymers: influence on cell-material interaction. *Plasma Chem Plasma Process* 32(5):1039–1073. doi:[10.1007/s11090-012-9394-8](https://doi.org/10.1007/s11090-012-9394-8)
21. Garcia JL, Asadinezhad A, Pachernik J, Lehocky M, Junkar I, Humpolicek P, Saha P, Valasek P (2010) Cell proliferation of HaCaT keratinocytes on collagen films modified by argon plasma treatment. *Molecules* 15(4):2845–2856. doi:[10.3390/molecules15042845](https://doi.org/10.3390/molecules15042845)
22. Gorjanc M, Mozetic M (2014) Modification of fibrous polymers by gaseous plasma: principles, techniques and applications. Lambert Academic Publishing, Saarbrücken
23. Kutasi K, Vasco G, Sa PA (2011) Active species downstream of an Ar–O₂ surface-wave microwave discharge for biomedicine, surface treatment and nanostructuring. *Plasma Sources Sci Technol* 20(3):035006. doi:[10.1088/0963-0252/20/3/035006](https://doi.org/10.1088/0963-0252/20/3/035006)
24. Vesel A, Kolar M, Doliska A, Stana-Kleinschek K, Mozetic M (2012) Etching of polyethylene terephthalate thin films by neutral oxygen atoms in the late flowing afterglow of oxygen plasma. *Surf Interface Anal* 44(13):1565–1571. doi:[10.1002/sia.5064](https://doi.org/10.1002/sia.5064)
25. Kregar Z, Biscan M, Milosevic S, Vesel A (2011) Monitoring oxygen plasma treatment of polypropylene with optical emission spectroscopy. *IEEE Trans Plasma Sci* 39(5):1239–1246. doi:[10.1109/Tps.2011.2123111](https://doi.org/10.1109/Tps.2011.2123111)
26. Belmonte T, Bernardelli EA, Mafra M, Duda D, Frache G, Poncin-Epaillard F, Noël C, Choquet P, Migeon HN, Maliska AM (2011) Comparison between hexatriacontane and stearic acid behaviours under late Ar–O₂ post-discharge. *Surf Coat Technol* 205(2):S443–S446. doi:[10.1016/j.surfcoat.2011.03.041](https://doi.org/10.1016/j.surfcoat.2011.03.041)
27. Belmonte T, Pintassilgo CD, Czerwiec T, Henrion G, Hody V, Thiebaut JM, Loureiro J (2005) Oxygen plasma surface interaction in treatments of polyolefines. *Surf Coat Technol* 200(1–4):26–30. doi:[10.1016/j.surfcoat.2005.02.108](https://doi.org/10.1016/j.surfcoat.2005.02.108)

28. Bernardelli EA, Mafrà M, Maliska AM, Belmonte T, Klein AN (2013) Influence of neutral and charged species on the plasma degradation of the stearic acid. *Mater Res* 16:385–391. doi:[10.1590/S1516-14392013005000008](https://doi.org/10.1590/S1516-14392013005000008)
29. Silva WD, Belmonte T, Duday D, Frache G, Noel C, Choquet P, Migeon HN, Maliska AM (2012) Interaction mechanisms between Ar–O₂ post-discharge and biphenyl. *Plasma Process Polym* 9(2):207–216. doi:[10.1002/ppap.201100119](https://doi.org/10.1002/ppap.201100119)
30. Mozetic M, Primc G, Vesel A, Zaplotnik R, Modic M, Junkar I, Recek N, Klanjšek-Gunde M, Guhy L, Sunkara MK, Assensio MC, Milosevic S, Lehocky M, Sedlarik V, Gorjanc M, Kutasi K, Stana-Kleinschek K (2015) Application of extremely non-equilibrium plasmas in the processing of nano and biomedical materials. *Plasma Sources Sci Technol* 24(1):015026. doi:[10.1088/0963-0252/24/1/015026](https://doi.org/10.1088/0963-0252/24/1/015026)
31. Zaplotnik R, Vesel A, Mozetic M (2011) Transition from E to H mode in inductively coupled oxygen plasma: hysteresis and the behaviour of oxygen atom density. *EPL Europhys Lett* 95(5):55001. doi:[10.1209/0295-5075/95/55001](https://doi.org/10.1209/0295-5075/95/55001)
32. Kortshagen U, Gibson ND, Lawler JE (1996) On the E–H mode transition in RF inductive discharges. *J Phys D Appl Phys* 29(5):1224–1236. doi:[10.1088/0022-3727/29/5/017](https://doi.org/10.1088/0022-3727/29/5/017)
33. Lee J-K, Lee H-C, Chung C-W (2011) E–H mode transition in inductively coupled plasma using Ar, O₂, N₂, and mixture gas. *Current Appl Phys* 11(5):S149–S153. doi:[10.1016/j.cap.2011.04.009](https://doi.org/10.1016/j.cap.2011.04.009)
34. Wang J, Du Y-C, Zhang X, Zheng Z, Liu Y, Xu L, Wang P, Cao J-X (2014) E → H mode transition density and power in two types of inductively coupled plasma configuration. *Phys Plasmas* 21(7):073502. doi:[10.1063/1.4886147](https://doi.org/10.1063/1.4886147)
35. Miyoshi Y, Petrovic ZL, Makabe T (2002) Transition between capacitive and inductive mode in inductively coupled plasma observed by emission computerized tomography. *IEEE Trans Plasma Sci* 30(1):130–131. doi:[10.1109/TPS.2002.1003958](https://doi.org/10.1109/TPS.2002.1003958)
36. Cunge G, Crowley B, Vender D, Turner MM (1999) Characterization of the E to H transition in a pulsed inductively coupled plasma discharge with internal coil geometry: bi-stability and hysteresis. *Plasma Sources Sci Technol* 8(4):576–586. doi:[10.1088/0963-0252/8/4/309](https://doi.org/10.1088/0963-0252/8/4/309)
37. Turner MM, Lieberman MA (1999) Hysteresis and the E–H transition in radiofrequency inductive discharge. *Plasma Sources Sci Technol* 8(2):312–324. doi:[10.1088/0963-0252/8/2/312](https://doi.org/10.1088/0963-0252/8/2/312)
38. Okigawa A, Tadokoro M, Itoh A, Nakano N, Petrovic ZL, Makabe T (1997) Three-dimensional optical emission tomography of an inductively coupled plasma. *Jpn J Appl Phys* 36(1):4605–4616. doi:[10.1143/JJAP.36.4605](https://doi.org/10.1143/JJAP.36.4605)
39. Okigawa A, Makabe T, Shibagaki T, Nakano N, Petrovic ZL, Kogawa T, Itoh A (1996) Robot assisted optical emission tomography in an inductively coupled plasma reactor. *Jpn J Appl Phys* 35(3):1890–1893. doi:[10.1143/JJAP.35.1890](https://doi.org/10.1143/JJAP.35.1890)
40. Pan J, Li G, Chen Z, Chen X, Zhu W, Xu K (2009) Alternative block polyurethanes based on poly(3-hydroxybutyrate-co-4-hydroxybutyrate) and poly(ethylene glycol). *Biomaterials* 30(16):2975–2984. doi:[10.1016/j.biomaterials.2009.02.005](https://doi.org/10.1016/j.biomaterials.2009.02.005)
41. Niu Y, Chen KC, He T, Yu W, Huang S, Xu K (2014) Scaffolds from block polyurethanes based on poly(*ε*-caprolactone) (PCL) and poly(ethylene glycol) (PEG) for peripheral nerve regeneration. *Biomaterials* 35(14):4266–4277. doi:[10.1016/j.biomaterials.2014.02.013](https://doi.org/10.1016/j.biomaterials.2014.02.013)
42. Kolar M, Mozetic M, Stana-Kleinschek K, Fröhlich M, Turk B, Vesel A (2015) Covalent binding of heparin to functionalized PET materials for improved haemocompatibility. *Materials* 8(4):1526. doi:[10.3390/ma8041526](https://doi.org/10.3390/ma8041526)
43. Schaber PM, Colson J, Higgins S, Thielen D, Anspach B, Brauer J (2004) Thermal decomposition (pyrolysis) of urea in an open reaction vessel. *Thermochim Acta* 424(1–2):131–142. doi:[10.1016/j.tca.2004.05.018](https://doi.org/10.1016/j.tca.2004.05.018)
44. Hearn MJ, Ratner BD, Briggs D (1988) SIMS and XPS studies of polyurethane surfaces. 1. Preliminary studies. *Macromolecules* 21(10):2950–2959. doi:[10.1021/ma00188a011](https://doi.org/10.1021/ma00188a011)
45. Shimizu K, Phanopoulos C, Loenders R, Abel ML, Watts JF (2010) The characterization of the interfacial interaction between polymeric methylene diphenyl diisocyanate and aluminum: a ToF-SIMS and XPS study. *Surf Interface Anal* 42(8):1432–1444. doi:[10.1002/sia.3586](https://doi.org/10.1002/sia.3586)
46. Shinohara H, Nakahara A, Kitagawa F, Takahashi Y, Otsuka K, Shoji S, Ohara O, Mizuno J (2011) XPS and NEXAFS studies of VUV/O₃ treated aromatic polyurea and its application to microchip electrophoresis. *Nanobiotechnol IET* 5(4):136–142. doi:[10.1049/iet-nbt.2011.0006](https://doi.org/10.1049/iet-nbt.2011.0006)
47. Moles MD, Scotchford CA, Campbell Ritchie A (2014) Oxidation state of a polyurethane membrane after plasma etching. *Conf Pap Sci* 2014:347979. doi:[10.1155/2014/347979](https://doi.org/10.1155/2014/347979)
48. Greenwood OD, Hopkins J, Badyal JPS (1997) Non-isothermal O₂ plasma treatment of phenyl-containing polymers. *Macromolecules* 30(4):1091–1098. doi:[10.1021/ma9604202](https://doi.org/10.1021/ma9604202)